Available online at www.sciencedirect.com
SCIENCE DIRECT®
Journal of Magnetic Resonance 169 (2004) 30–38
JMR Journal of Magnetic Resonance
www.elsevier.com/locate/jmr

The effect of rotational angle and experimental parameters on the diffraction patterns and micro-structural information obtained from *q*-space diffusion NMR: implication for diffusion in white matter fibers

Liat Avram,[a] Yaniv Assaf,[a,b] and Yoram Cohen[a,*]

[a] *School of Chemistry, The Sackler Faculty of Exact Sciences, Tel Aviv University, Ramat Aviv, Tel Aviv 69978, Israel*
[b] *Department of Radiology, The Wohl Institute for Advanced Imaging, Tel Aviv Sourasky Medical Center, Tel Aviv 64239, Israel*

Received 7 July 2003; revised 6 January 2004
Available online 27 April 2004

Abstract

Diffusion NMR may provide, under certain experimental conditions, micro-structural information about confined compartments totally non-invasively. The influence of the rotational angle, the pulse gradient length and the diffusion time on the diffusion diffraction patterns and *q*-space displacement distribution profiles was evaluated for ensembles of long cylinders having a diameter of 9 and 20 μm. It was found that the diffraction patterns are sensitive to the rotational angle (α) and are observed only when diffusion is measured nearly perpendicular to the long axis of the cylinders i.e., when $\alpha = 90° \pm 5°$ under our experimental conditions. More importantly, we also found that the structural information extracted from the displacement distribution profiles and from the diffraction patterns are very similar and in good agreement with the experimental values for cylinders of 20 μm or even 9 μm, when data is acquired with parameters that satisfy the short gradient pulse (SGP) approximation (i.e., $\delta \to 0$) and the long diffusion time limit. Since these experimental conditions are hardly met in in vitro diffusion MRI of excised organs, and cannot be met in clinical MRI scanners, we evaluated the effect of the pulse gradient duration and the diffusion time on the structural information extracted from *q*-space diffusion MR experiments. Indeed it was found that, as expected, accurate structural information, and diffraction patterns are observed when Δ is large enough so that the spins reach the cylinders' boundaries. In addition, it was found that large δ results in extraction of a compartment size, which is smaller than the real one. The relevance of these results to *q*-space MRI of neuronal tissues and fiber tracking is discussed.

1. Introduction

Diffusion NMR and MRI are important tools for studying porous media and biological tissues [1–3]. In recent years diffusion has become an important contrast mechanism in MRI of neuronal tissues, where applications range from fiber mapping to detection of a variety of diseases [4–13]. Whereas *k*-space imaging provides maps of molecular spin density, *q*-space analysis of diffusion data yields information on the molecular displacement probability, i.e., the diffusion propagator. In the case of restricted diffusion, the displacement probability is affected by the structural characteristics of the confining compartment in which the diffusion is sampled [14]. In fact, in the limit of long diffusion time, where all molecules sample the entire confining compartment, the displacement distribution profile becomes an autocorrelation function of the spin density [15]. For well-defined systems, diffraction-like patterns were predicted and found for various systems when the signal decay was plotted against the reciprocal space vector q defined as $\gamma G\delta/2\pi$. Here, γ is the magnetogyric ratio, G is the gradient strength, and δ is the duration of the pulsed gradients. It was shown that these diffraction patterns provide a means of obtaining the size and shapes of the confined compartments in which the diffusion occurs [16–21].

* Corresponding author. Fax: +972-3-6409293.
E-mail address: ycohen@post.tau.ac.il (Y. Cohen).

1090-7807/$ - see front matter © 2004 Elsevier Inc. All rights reserved.
doi:10.1016/j.jmr.2004.03.020

King et al. [22,23] applied q-space diffusion MRS to study cerebral ischemia in mice brain and Kuchel et al. [24–26] were able to show that diffraction-like patterns can be observed, in vitro, in red blood cells that are characterized by a relatively regular size, and shape. Recently, we have combined q-space diffusion with k-space MR imaging with the aim of mapping the displacement distribution profiles in each pixel in heterogeneous neuronal systems such as the spinal cord and human brain [27–31]. As neuronal tissues are much less regular systems as compared to porous media or even red blood cells, diffraction patterns were not clearly visible in these systems, at least when water diffusion was measured in those neuronal tissues. In these neuronal systems, the structural information was obtained from the Fourier transform of the signal decay as a function of q, as suggested by Cory and Garroway [32]. However, in order to obtain sufficient q-space resolution for characterization of small compartments sampling at high q-values is required. Therefore, in q-space diffusion weighted MRI (DWI), high q-values are usually obtained by long diffusion gradient pulses for which the short gradient pulse (SGP) approximation (i.e., $\delta \to 0$) is violated. In some cases, even the long diffusion time limit i.e., the condition in which $\Delta \gg l^2/2D$ (where l is the size of the compartment in which spins with diffusion coefficient D are diffusing), is hardly met. In clinical DWI the condition in which $\Delta \gg \delta$ is also often not fulfilled.

Diffusion tensor MRI (DTI) is increasingly used to map fiber orientation, connection, and directionality by exploiting the fact that water diffusion in CNS fibers appears anisotropic. Here, the main concern is to find the direction of the highest diffusivity. However, it was found that this is not an easy task for pixels or voxels with crossing fibers and where a complex network of fibers exist [11–13].

We therefore decided to explore the effect of the rotational angle (α), the diffusion time and the pulse gradient length on the diffraction pattern and the structural information extracted from q-space diffusion NMR. This structural information was extracted from the diffraction pattern, when apparent, and more importantly from the displacement distribution profiles obtained by Fourier transform of the signal decays. We chose to study ensembles of long open cylinders having a diameter of 20 and 9 μm that are characterized by a narrow size distribution, but the sizes of which are relevant to the cylindrical structures found in neuronal tissues. A good agreement was found between the structural information obtained from the two methods of analysis. The rotational angle (α), i.e., the angle between the main axis of the cylinders and the diffusion gradients direction as shown in Fig. 1, was found to have a pronounced effect on the diffraction-like patterns implying that the diffusion diffractions, and the displacement distribution profiles extracted thereof are indeed good markers for restricted diffusion.

In addition, the diffusion time, $(\Delta - \delta/3)$, and the pulse gradient duration, δ, were found to have a pronounced effect on the appearance of the diffraction pattern and on the accuracy of the structural information obtained from the above methods of analysis. The relevance of above observations to the extraction of structural information in neuronal tissues and fiber orientation in the CNS is briefly discussed.

2. Experimental section

NMR diffusion experiments were performed on ensembles of hollow cylindrical tubes having an inner diameter of 9 and 20 μm and an outer diameter of 150 μm. (Polymicro Technologies, USA part Nos. 2000004(TSP010150) and 2000008(TSP020150), respectively.) These NMR diffusion experiments were collected on a 8.4 T Bruker–Avance NMR spectrometer equipped with a Micro5 gradient system capable of producing pulse gradients of up to 190 G cm^{-1} in each of the three directions. The fibers were cut into tubes of 4.5 ± 0.5 cm in length and filled with water and aligned along the z direction in the magnet. The tubes were first aligned in a 4 mm NMR tube which was inserted into a 5 mm NMR tube. For the angle dependence experiments we also prepared tubes of 1.5 ± 0.1 and 0.9 ± 0.1 cm, which were placed in the center of the RF and the gradient coils.

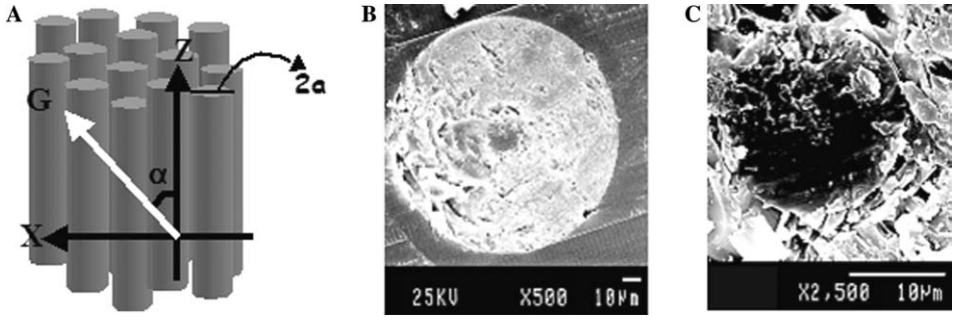

Fig. 1. (A) Schematic representation of the sample studied and determination of the rotational angle (α) between the main axis of the cylinders and the diffusion gradients direction. (B and C) Electron micrographs of the 20 μm tubes at two different magnifications.

NMR diffusion measurements were performed using the stimulated echo diffusion sequence [33]. The following parameters were used for the 20 μm cylindrical tubes: TR = 4.2 s, TE = 20 ms, $\delta = 2$ ms, and Δ of 1000 ms. The diffusion was measured for different angles from the +z-direction (0°) to the −z-direction (180°). The following rotational angles (αs) were sampled: 0°, 45°, 67.5°, 78.7°, 84.4°, 88°, 90°, 92°, 95.6°, 101.3°, 112.5°, 135°, and 180°. For $\alpha = 0°$, 45°, 67.5°, 112.5°, 135°, and 180°, G was incremented to 45 G cm^{-1} in 16 steps while, for all other angles, G was incremented to 160 G cm^{-1} in 32 equal steps. For $G_{max} = 160$ G cm^{-1}, the resulting q_{max} and b_{max} were 1274 cm^{-1} and 7.32×10^7 s cm^{-2}, respectively. For the 1.5 ± 0.1 cm tubes the following angles were sampled: 90°, 88°, 85°, 80°, 67°, and 82° while only 80° and 90° were sampled for the 0.9 ± 0.1 cm tubes. These diffusion experiments were performed with the above parameters.

For the 9 μm tubes the same diffusion sequence was used with the following parameters: TR = 3.6 s, TE = 22 ms, $\delta = 3$ ms, and Δ of 400 ms. The following rotational angles (αs) were sampled: 0°, 45°, 78.7°, 84.4°, 88°, 90°, and 180°. For $\alpha = 0°$, 45°, and 180°, G was incremented to 45 G cm^{-1} in 16 steps while for $\alpha = 78.7°$, 84.4°, 88°, and 90°, G was incremented to 160 G cm^{-1} in 32 equal steps. For $G_{max} = 160$ G cm^{-1}, the resulting q_{max} and b_{max} were 1911 cm^{-1} and 6.58×10^7 s cm^{-2}, respectively.

In the 20 μm cylinders for $\alpha = 90°$, we evaluated the effect of the diffusion time on the observed diffractions. In these experiments the PGSTE sequence was used with the above parameters while Δ had the following values: 1000, 500, 200, 100, 50, 30, and 15 ms. To evaluate the effect of the violation of the SGP approximation on the diffraction pattern and the structural information extracted from the displacement distribution profiles, water diffusion was measured with the PGSTE sequence for $\alpha = 90°$ with the following pairs of gradient duration (δ) and maximal gradient strength (G_{max}): $\delta = 2$ ms, $G_{max} = 160$ G cm^{-1}; $\delta = 4$ ms, $G_{max} = 80$ G cm^{-1}; $\delta = 8$ ms, $G_{max} = 40$ G cm^{-1}; $\delta = 16$ ms, $G_{max} = 20$ G cm^{-1}; $\delta = 32$ ms, $G_{max} = 10$ G cm^{-1}; $\delta = 64$ ms, $G_{max} = 5$ G cm^{-1}. For the 9 μm cylinders the following pairs of gradient duration (δ) and maximal gradient strength (G_{max}) were used: $\delta = 3$ ms, $G_{max} = 160$ G cm^{-1}; $\delta = 6$ ms, $G_{max} = 80$ G cm^{-1}; $\delta = 12$ ms, $G_{max} = 40$ G cm^{-1}; $\delta = 24$ ms, $G_{max} = 20$ G cm^{-1}; $\delta = 48$ ms, $G_{max} = 10$ G cm^{-1}.

3. Results

3.1. The effect of the rotational angle (α) on the diffraction pattern and on the structural information extracted from the displacement distribution profile

Figs. 2A and B show the signal decay for an ensemble of 4.5 ± 0.5 cm long cylinders having a diameter of 20 μm as a function of the gradient strength, G, for two rotational angles, (αs), 90°, and 84.4°, respectively. These spectra, which were acquired with exactly the same experimental parameters, clearly demonstrate that a diffraction-like pattern is observed only in the case of $\alpha = 90°$.

Figs. 3A–C show the same data for 1.5 ± 0.1 cm long cylinders having a diameter of 20 μm placed in the center of the RF and gradient coils. Here, some diffraction was

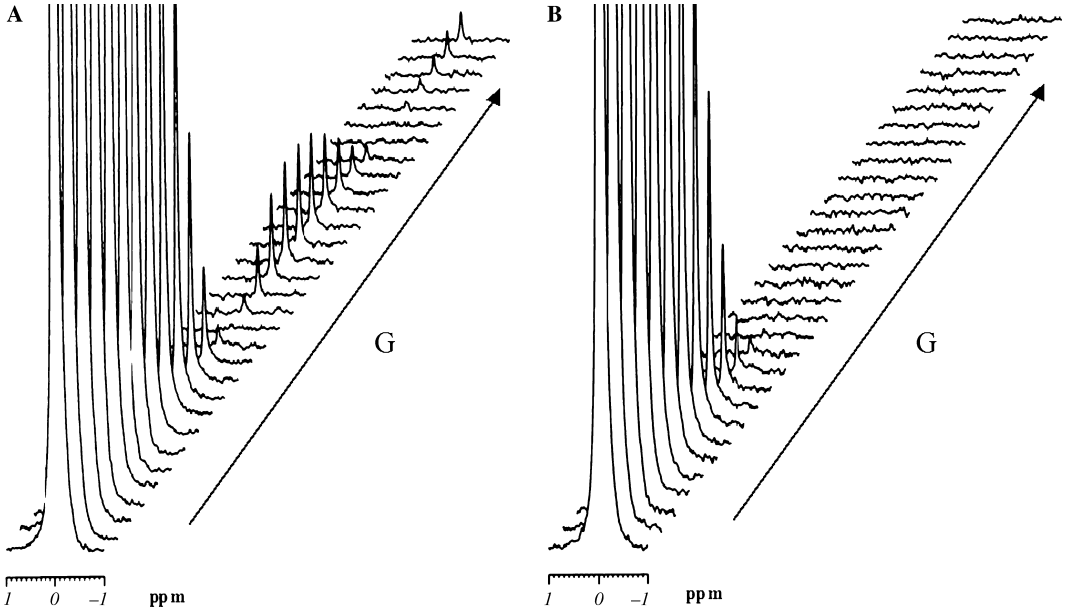

Fig. 2. ^{1}H NMR signal decay as a function of the gradient strength (G) for water in 20 μm cylinders having a length of 4.5 ± 0.5 cm for the rotational angles (αs) of: (A) 90° and (B) 84.4°.

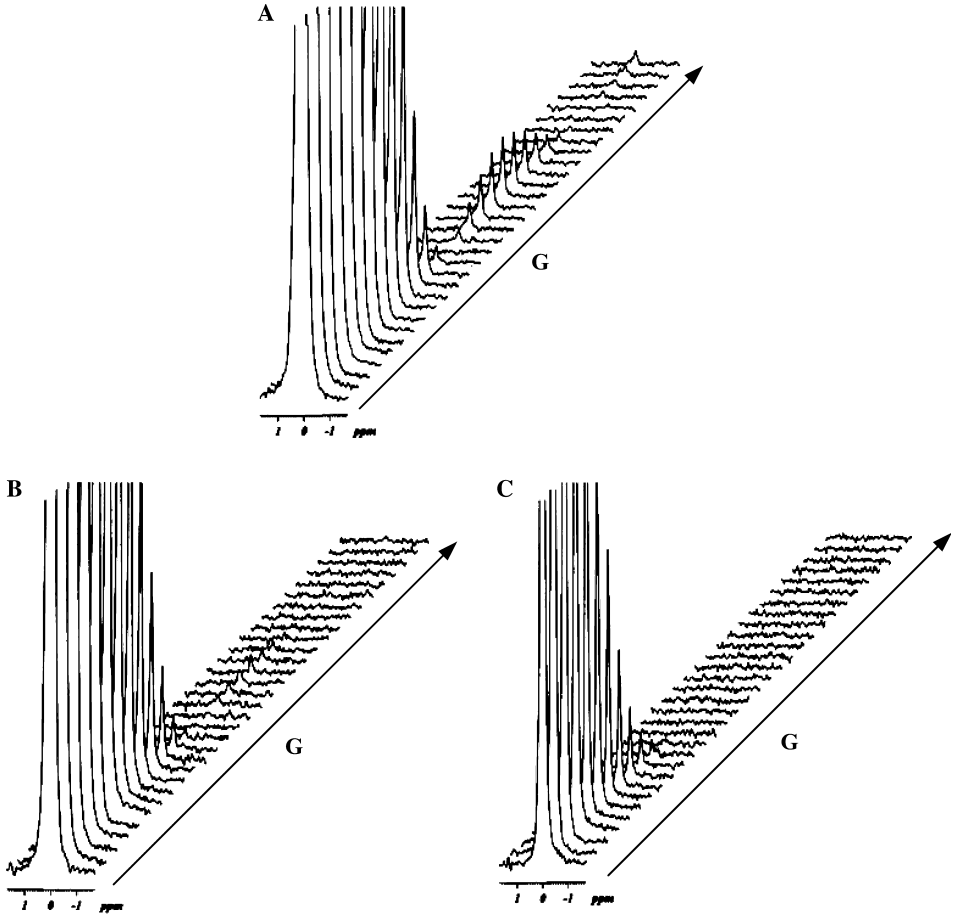

Fig. 3. ^{1}H NMR signal decay as a function of the gradient strength (G) for water in 20 μm cylinders having a length of 1.5 ± 0.1 cm for the rotational angles (αs) of: (A) 90°, (B) 85°, and (C) 82°.

obtained when $\alpha = 85°$, but no diffraction was observed for $\alpha = 82°$.

Figs. 4A and B depict the signal decay as a function of the q-values for the different rotation angles studied in the case of 20 μm cylinders of 4.5 ± 0.5 and 1.5 ± 0.1 cm of length, respectively. Diffractions were observed for the ensembles of the 20 μm cylinders having a length of 4.5 ± 0.5 cm only when the diffusion was measured

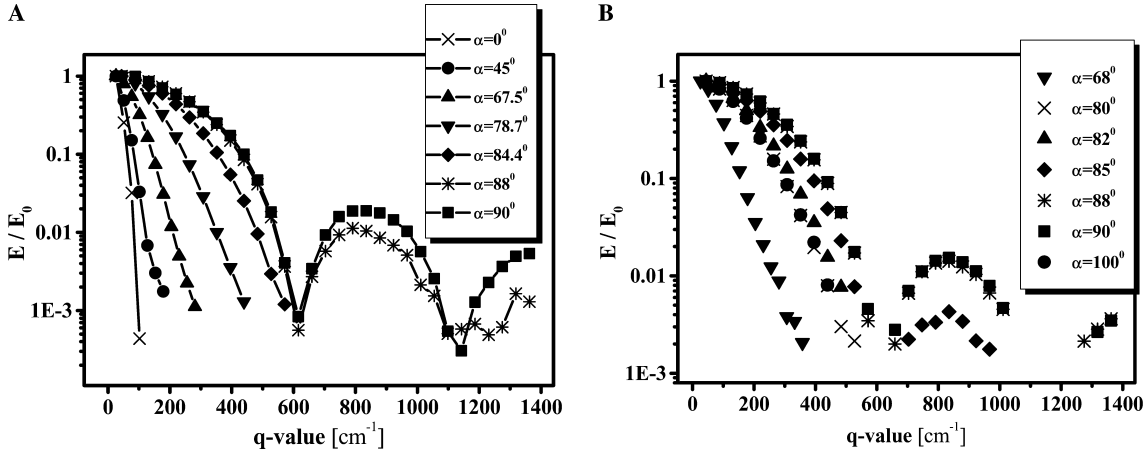

Fig. 4. Normalized signal decay as a function of the q-values for the different rotational angles (αs) for ensembles of 20 μm cylinders having a length of: (A) 4.5 ± 0.5 cm and (B) 1.5 ± 0.1 cm. The results for the rotation angles ($180° - \alpha$) were identical to those obtained for α and are therefore not shown.

nearly perpendicular (i.e., when α was 90°, 88°, and 92°) to the long axis of the cylinders. In the case of the 1.5 ± 0.1 cm long cylinders that were placed in the center of the RF and gradient coils a very weak diffraction was also observed when $\alpha = 85°$ (Fig. 4B). It was found, as expected, that the actual diameters of the cylinders can be obtained from the diffractions.

When the decay curve for the 20 μm cylinders at $\alpha = 90°$ was compared with the prediction of Callaghan's formula for restricted diffusion in cylinders [19], very good agreement was found between the experimental values, and the simulated values as shown in Fig. 5.

Here, the data for the 20 μm cylinders ($\alpha = 90°$) were obtained with δ and Δ of 2 and 1000 ms, respectively implying that both the SGP approximation and the long diffusion time limit are met or at least approached. Consequently, there is very good agreement between the experimental and simulated data. From the first minima of $E_{(\Delta,q)}$ vs. q ($q_{\min}$) it was possible to extract the diameter of the cylinders. Indeed, $1.22/q_{\min}$, as suggested by Callaghan [19], gives a value of 19.8 μm, which is in good agreement with the 20 μm value expected. Structural information can also be extracted from the displacement distribution profiles obtained from the Fourier transform of the signal decay as a function of q-values [32]. Fig. 6 shows the displacement distribution profiles obtained from the signal decay of water in the 20 μm tubes for the different rotational angles. The numerical values obtained from this analysis are shown in Table 1.

It was found that, as expected, the minimal displacement is indeed obtained when $\alpha = 90°$. More importantly, we found that $1.22\Delta X_{0.5}$, when $\Delta X_{0.5}$ is the full width of the displacement distribution profile at half-height (FWHH), generates the diameter of the cylinders at least in the case of the 20 μm cylindrical tubes when $\alpha = 90° \pm 2°$. For the 9 μm tubes, however, the extracted diameter was smaller than the expected

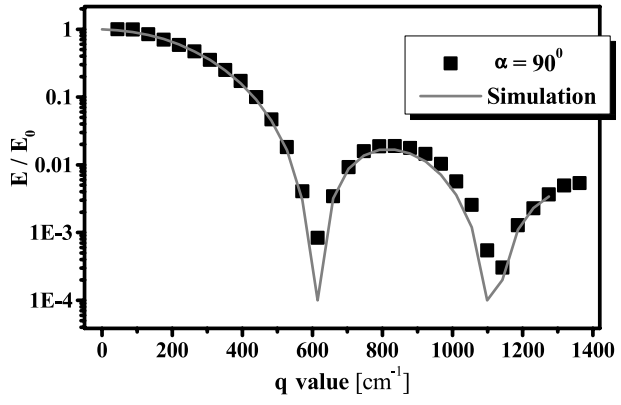

Fig. 5. Experimental and simulated normalized signal decay as a function of the q-values for the 20 μm cylinders. Simulations were performed using the formula given in [19].

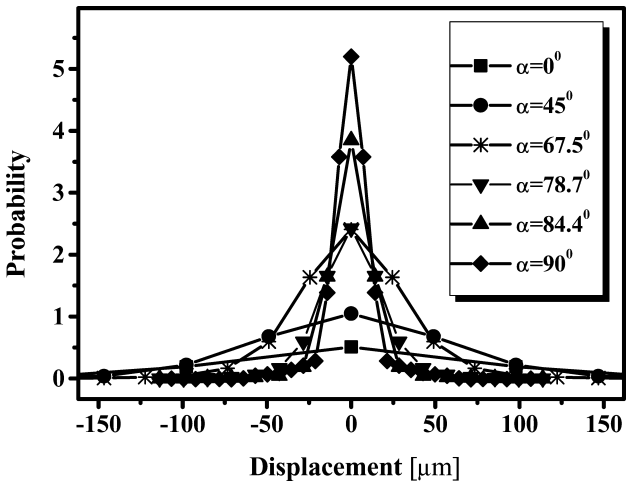

Fig. 6. Displacement distribution profiles for the 20 μm cylinders as a function of the rotational angles (αs).

9μm and was found to be 7.1 and 7.2 μm for the value extracted from the diffraction ($1.22/q_{\min}$), and displacement distribution profile ($1.22\Delta X_{0.5}$), respectively. Since the deviation was observed in the two methods used, we assumed that the deviation originates from the fact that the SGP approximation is violated to a greater extent in the case of the 9 μm cylindrical tubes even when δ was only slightly larger i.e., 3 ms. In diffusion MRI of in vivo systems, certainly when the data are acquired with clinical scanners, where the diffusion weighting is obtained from large δ, this effect may be even more pronounced. This effect may be even larger in biological systems where many of the compartments are smaller than 9 μm. We therefore decided to evaluate the effect of the diffusion time and pulse gradient duration (δ) on the diffraction pattern and on the structural parameters extracted from the displacement distribution profiles as will be described in the next section.

3.2. The effect of the diffusion time ($\Delta - \delta/3$) and pulse gradient length (δ) on the diffraction pattern and extracted structural information

The extraction of structural information from the q-space analysis of MR diffusion data was derived first for the SGP approximation in the long diffusion time limit. When we measured the signal decay in the 20 μm cylinders for $\alpha = 90°$ as a function of the diffusion time we indeed found that the diffraction-like pattern appears less pronounced when the diffusion time decreased as shown in Fig. 7. In these experiments the pulse gradient duration, δ, was 2 ms.

It should be noted that very similar results were also obtained for $\alpha = 88°$ (data not shown). We found as in previous reports [18,19], that very pronounced diffraction patterns have already been observed for diffusion times in the order of $l^2/2D$ and not only when $\Delta \gg l^2/2D$.

Table 1
Structural parameters extracted from the full width at half-height (FWHH) of the displacement distribution profiles and the apparent diffusion coefficient (ADC) as a function of the rotational angle (α), for the 20 and 9 μm cylinders[a]

α		0°	45°	67.5°	78.7°	840.4°	88°	90°
20 μm	$\Delta X_{0.5}$ (μm)	142.4	108.5	58.1	33.7	21.9	17.5	16.9
	$1.22 \cdot \Delta X_{0.5}$ (μm)	173.7	132.4	70.9	41.1	26.7	21.3 (19.8)[b]	20.6 (19.8)[b]
	$0.425 \cdot \Delta X_{0.5}$ (μm)	60.5	46.1	24.7	14.3	9.3	7.4	7.1
	ADC[c]($\times 10^{-5}$ cm^2 s^{-1})	1.991	0.812	0.263	0.094	0.048	0.031	0.028
	$(2*ADC*t_d)^{0.5}$[c](μm)	63.1	40.3	22.9	13.7	9.8	7.9	7.5
9 μm	$\Delta X_{0.5}$ (μm)	91.5	69.9	—	18.6	10.0	6.7	5.9
	$1.22 \cdot \Delta X_{0.5}$ (μm)	111.7	85.3	—	22.7	12.2	8.2 (7.1)[b]	7.2 (7.1)[b]
	$0.425 \cdot \Delta X_{0.5}$ (μm)	38.9	29.7	—	7.9	4.3	2.8	2.5
	ADC[c] ($\times 10^{-5}$cm^2 s^{-1})	1.842	0.914	—	0.075	0.026	0.012	0.009
	$(2*ADC*t_d)^{0.5}$[c](μm)	38.4	27.0	—	7.7	4.6	3.1	2.7

[a] The values of Δ and δ were 1000 and 2 ms for the 20 μm cylinders and 400 and 3 ms for the 9 μm cylinders, respectively.
[b] Size extracted from the first minima of diffraction pattern (q_{min} taken as $1.22/q_{min}$).
[c] ADCs were calculated from the linear part of the signal decay of each curve.

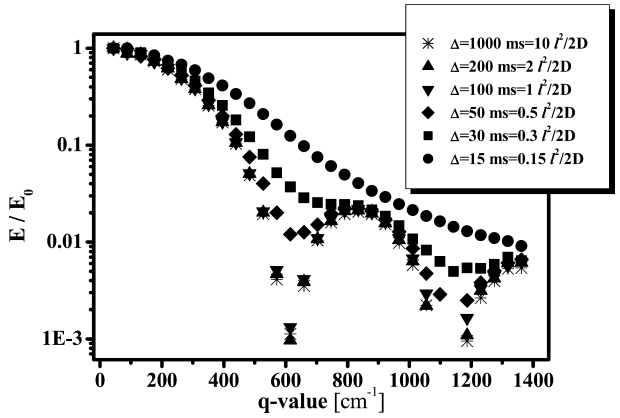

Fig. 7. Normalized signal decay for the 20 μm cylinders at a rotational angle α of 90° as a function of the q-values for different diffusion times. The pulse gradient length, δ, was 2 ms.

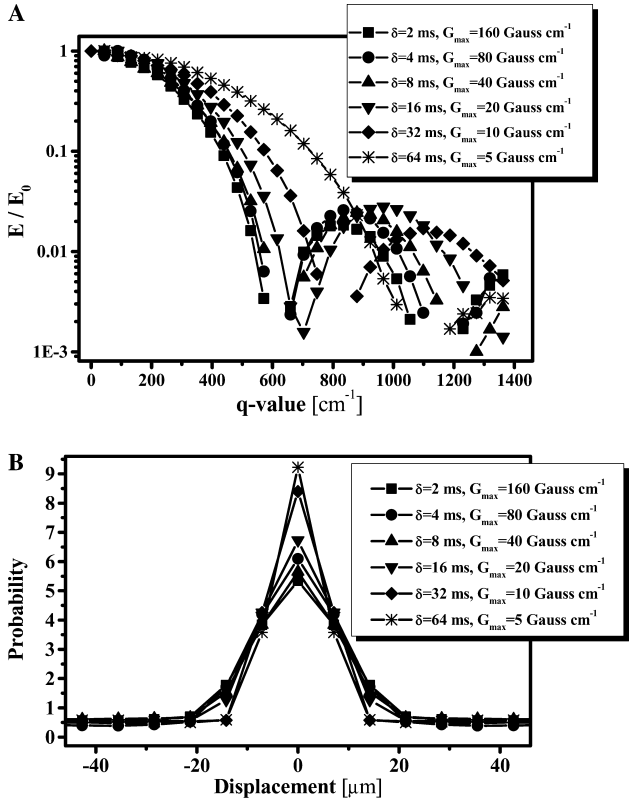

Fig. 8. The effect of the pulse gradient duration (δ) (in the long diffusion time limit) for the 20 μm cylinders for $\alpha = 90°$ on: (A) the normalized signal decay as a function of q, and on (B) the displacement distribution profiles obtained from FT of the data shown in (A).

The effect of the violation of the SGP approximation on the diffraction pattern and on the structural information extracted from the displacement distribution profile was obtained by repeating the diffusion experiments where the pair of parameters δ and G_{max} were changed in a way that kept q_{max} constant. Fig. 8A shows the signal decay as a function of the q-values for the different diffusion experiments performed with the different pairs of δ and G_{max}, while Fig. 8B shows the displacement distribution profiles obtained from the FT of the data shown in Fig. 8A. The numerical values obtained from these analyses for the 20 and the 9 μm cylinders are summarized in Table 2.

It was found that as δ is increased and the SGP approximation is violated, the diffraction moves to higher q, as predicted before by simulations [34], and the displacement profile narrows thus indicating that the diameter that would be extracted from these analyses would indeed be smaller than the real diameter of the confined compartment. For the 20 μm cylinders it was found that the deviation in the extracted diameter is less than a factor of 2 when δ is increased by a factor of 32 from 2 to 64 ms. However, for the 9 μm cylinders the deviation in the extracted diameter with the increase in δ was found to be much more pronounced (Table 2).

Table 2
The effect of violation of the SGP approximation on the structural information extracted from the FWHH ($\Delta X_{0.5}$) of the displacement distribution profiles for $\alpha = 90°$

G (G cm^{-1})/δ (ms)		160/2	80/4	40/8	20/16	10/32	5/64
20 μm	$\Delta X_{0.5}$ (μm)	16.9	16.4	15.5	14.2	11.4	9.8
	$1.22{\cdot}\Delta X_{0.5}$ (μm)	20.6	20.0	18.9	17.3	13.9	12.0
G (G cm^{-1})/δ (ms)		160/3	80/6	40/12	20/24	10/48	
9 μm	$\Delta X_{0.5}$ (μm)	5.9	4.9	3.8	1.8	1.6	
	$1.22{\cdot}\Delta X_{0.5}$ (μm)	7.2	6.0	4.6	2.2	2.0	

4. Discussion and conclusions

In recent years it became apparent that, at sufficiently high diffusion weighting, the water signal decay in neuronal tissues is not mono-exponential [20,35–40]. In fact, at least in white matter rich areas, there is a certain water population that seems to exhibit restricted diffusion in some directions [11–13,27–31,35–40]. As q-space analysis of NMR diffusion data is a useful means for detecting restricted diffusion it was suggested as a viable approach to analyze high b-value DWI data at least in white matter. In addition, using specific experimental conditions, the q-space approach may be used for obtaining structural information of the neuronal tissues [21,22,27–31]. In contrast to homogeneous periodic samples, diffraction patterns are not observed in neuronal tissues, probably because of size heterogeneity [39], and exchange [26]. Therefore, in these tissues the structural information should be obtained by computing the displacement distribution profiles from the Fourier transform of the signal decay versus q, as previously suggested [32].

In the present study, long micro-cylinders, of precise diameters, were used as a model of white matter fibers. Using this model we were able to demonstrate that the structural information obtained from the diffraction peaks and the displacement distribution profiles provides very similar results that are in very good agreement with the actual sizes of the 9–20 μm cylinders. For smaller compartments in the range of ~5 μm it is clear that the extracted sizes, although not tested experimentally, will be smaller than the real ones, even when operating with relatively strong gradient systems. This deviation is expected to be more pronounced when such analysis is performed on MR diffusion data acquired with clinical scanners where diffusion weighting is mainly achieved by using relatively long pulse gradients (i.e., δ in the order of tens of milliseconds). There, as previously pointed out, the extracted mean displacements are only apparent displacements [30,31]. For the sciatic nerve for example it has previously been shown that changing the δ and $G_{\max}$ pair from 4.5 ms and 160 G cm^{-1} to 72 ms and 10 G cm^{-1}, respectively resulted in a decrease by a factor of two in the averaged apparent mean displacement [30]. These results are in accordance with the prediction of previously reported simulations [34]. This means that there are deviations in absolute values, however the trend in the values and the relative sizes of the apparent mean displacements is maintained, and therefore may be used as a diagnostic tool as previously demonstrated [30,31]. Table 1 also shows that, for rotational angles very different from 90°, the mean displacements obtained from the Einstein equation using the ADCs extracted by fitting the linear part of the signal decay and from the $0.425\Delta X_{0.5}$ relation afford similar mean displacement for the water molecules as expected for free diffusion [32]. For $\alpha = 90° \pm 2°$, it is $1.22\Delta X_{0.5}$ that provides the actual size of the cylinders.

A somewhat surprising result of this study is the relative sensitivity of the diffusion diffraction pattern on the rotational angle (α). For the long tubes, diffractions were observed only for $\alpha = 90° \pm 2°$. For the shorter tubes of 1.5 ± 0.1 cm of length, placed in the center of the RF and gradient coils, diffraction patterns were observed for α in the range of 85°–95°, i.e., when the diffusion is measured nearly perpendicular to long axis of the cylinder. The more pronounced dependency of the diffraction pattern in the case of the 4.5 cm tubes probably originates from the non-linearity of the gradient coils over the length of the tubes. To further verify this point tubes of 0.9 ± 0.1 cm in length, placed in the center of the RF and gradient coils, were measured. There, no diffraction was observed for $\alpha = 80°$. This suggests that one can use diffusion diffraction to reveal the perpendicular axis of the cylinder and hence to use it to determine the principal axis of the cylinder along which the diffusion is maximal by simple rotation. Therefore such a diffraction, if observed in biological tissues, may assist in the determination of the most restricted direction from which one should be able to find the direction of the maximal diffusivity. However, as stated before, diffusion diffractions are not observed in neuronal tissues, probably due to size distribution [39], and exchange [26]. Peled et al. [39] have shown that the apparent multi-exponential signal decay observed in neuronal tissues is in fact the sum of many diffractions from axons with different sizes. Therefore, in such tissues one has to resort to the displacement distribution profile, which is efficient at characterizing the apparent slow diffusing

component that was found to be sensitive to the direction of the applied diffusion gradients [27–31]. The sharpest profile may thus indicate the most restricted direction from which the main diffusivity can, in principle, be determined by a simple rotation. Such an approach may provide good means for following the main diffusivity in connected cylinders and may provide a more robust means for following fibers. It should be noted that the effect of the rotational angles on ADCs in 50 μm tubes was recently reported [41].

The present study demonstrates that the micro-cylinders may in fact be used as a model system for better understanding diffusion in fibers that bear some relevance to the kind of diffusion observed in white matter fibers in the CNS. Both the diffractions, when observed, and more importantly the displacement distribution profiles provide very similar structural information that is in good agreement with the real physical size of the compartments. In addition, we found that diffraction patterns of sufficient intensity are observed even for relatively regular system, only within a narrow range of rotational angles, i.e., when the diffusion is measured nearly perpendicular to long axis of the cylinders. To further explore the ability to extract structural information from high *b*-value DWI, and its dependency on the rotation angle, as an indicator for the fiber directionality we also plan to study these cylinders by adding an extra-cylindrical space and by challenging the above approach with crossing fibers.

Acknowledgments

We thank the referees for their helpful comments. Financial support from The Israel Science Foundation (ISF Grant No. 522/03) founded by The Israel Academy of Sciences and Humanities is greatfully acknowledged. The authors wish to thank Ms. Inbal E. Biton for her help.

References

[1] P.T. Callaghan, Principles of Nuclear Magnetic Resonance Microscopy, Clarendon Press, Oxford, 1991.
[2] D. Le Bihan, Diffusion and Perfusion Magnetic Resonance Imaging, Raven Press, NY, 1995.
[3] Y. Cohen, M. Neeman (Eds.), Diffusion NMR and MRI: Basic Concepts and Applications, Israel J. Chem. 43 (2003) 1–164.
[4] M.E. Moseley, Y. Cohen, J. Mintorovitch, L. Chileuitt, H. Shimizu, J. Kucharczyk, M.F. Wendland, P.R. Weinstein, Early detection of regional cerebral ischemia in cats-comparison of diffusion-weighted and T2-weighted MRI and spectroscopy, Magn. Reson. Med. 14 (1990) 330–346.
[5] P.W. Schaefer, P.E. Grant, R.G. Gonzalez, Diffusion-weighted MR imaging of the brain, Radiology 217 (2000) 331–345.
[6] M. Eis, T. Els, M. Hoehn-Berlage, High-resolution quantitative relaxation and diffusion MRI of three different experimental brain tumors in rat, Magn. Reson. Med. 34 (1995) 835–844.
[7] D.C. Alsop, H. Murai, J.A. Detre, T.K. McIntosh, D.H. Smith, Detection of acute pathologic changes following experimental traumatic brain injury using diffusion-weighted magnetic resonance imaging, J. Neurotrauma 13 (1996) 515–521.
[8] Y. Assaf, A. Holokovsky, E. Berman, Y. Shapira, E. Shohami, Y. Cohen, Diffusion and perfusion magnetic resonance imaging following closed head injury in rats, J. Neurotrauma 16 (1999) 1165–1176.
[9] K. Takano, L.L. Latour, J.E. Formato, R.A.D. Carano, K.G. Helmer, Y. Hasegawa, C.H. Sotak, M. Fisher, The role of spreading depression in focal ischemia evaluated by diffusion mapping, Ann. Neurol. 39 (1996) 308–318.
[10] M. Cercigani, G. Iannuci, M.A. Rocca, G. Comi, M.A. Horsfield, M. Filippi, Pathologic damage in MS assessed by diffusion-weighted and magnetization transfer MRI, Neurology 54 (2000) 1139–1144.
[11] P.J. Basser, J. Mattiello, D. LeBihan, MR diffusion tensor spectroscopy and imaging, Biophys. J. 66 (1994) 259–267.
[12] P.J. Basser, S. Pajevic, C. Pierpaoli, J. Duda, A. Aldroubi, In vivo tractography using DT-MRI data, Magn. Reson. Med. 44 (2000) 625–632.
[13] P.C. van Zijl, D. Le Bihan, (Eds.), Diffusion tensor imaging and axonal mapping—state of art, NMR Biomed. 15 (2002) 431–593.
[14] J. Kärger, W. Heink, The propagator representation of molecular transport in microporous crystallites, J. Magn. Reson. 51 (1983) 1–7.
[15] P.T. Callaghan, D. MacGowan, K.J. Packer, F.O. Zelaya, High-resolution *q*-space imaging in porous structures, J. Magn. Reson. 90 (1990) 177–182.
[16] P.T. Callaghan, A. Coy, T.P.J. Halpin, D. MacGowan, K.J. Packer, F.O. Zelaya, Diffusion in porous systems and the influence of pore morphology in pulsed gradient spin-echo nuclear magnetic resonance studies, J. Chem. Phys. 97 (1992) 651–662.
[17] M. Appel, G. Fleischer, D. Geschke, J. Kärger, M. Winkler, Pulsed-field-gradient NMR analogue of the single-slit diffraction pattern, J. Magn. Reson. A 122 (1996) 248–250.
[18] S.J. Gibbs, Observation of diffusive diffraction in a cylindrical pore by PFG NMR, J. Magn. Reson. 124 (1997) 223–226.
[19] P.T. Callghan, Plused-gradient spin echo NMR for planar, cylindrical and spherical pores under conditions of wall relaxation, J. Magn. Reson. A 113 (1995) 53–59.
[20] B. Håkansson, R. Pons, O. Söderman, Diffraction-like effects in a highly concentrated W/O emulsion: a PFG NMR study, Magn. Reson. Imaging 16 (1998) 643–646.
[21] D. Topgaard, O. Söderman, Experimental determination of pore shape and size using *q*-space NMR microscopy in the long diffusion-time limit, Magn. Reson. Imaging 21 (2003) 69–76.
[22] M.D. King, J. Houseman, S.A. Roussel, N. van Bruggen, S.R. Williams, D.G. Gadian, *q*-Space imaging of the brain, Magn. Reson. Med. 32 (1994) 707–713.
[23] M.D. King, J. Houseman, D.G. Gadian, A. Connelly, Localized *q*-space imaging of the mouse brain, Magn. Reson. Med. 38 (1997) 930–937.
[24] P.W. Kuchel, A. Coy, P. Stilbs, NMR "diffusion-diffraction" of water revealing alignment of erythrocytes in a magnetic field and their dimensions and membrane transport characteristics, Magn. Reson. Med. 37 (1997) 637–643.
[25] P.W. Kuchel, C.J. Durrant, Permeability coefficients from NMR *q*-space data: models with unevenly spaced semi-permeable parallel membranes, J. Magn. Reson. 139 (1999) 258–272.
[26] A.M. Torres, R.J. Michniewicz, B.E. Chapman, G.A.R. Young, P.W. Kuchel, Characterization of erythrocyte shapes and sizes by NMR diffusion-diffraction of water: correlations with electron micrographs, Magn. Reson. Imaging 16 (1998) 423–434.

[27] Y. Assaf, Y. Cohen, Assignment of the water slow diffusing component in CNS using *q*-space diffusion MRS: implications to fiber tract imaging, Magn. Reson. Med. 43 (2000) 191–199.

[28] Y. Assaf, A. Mayk, Y. Cohen, Displacement imaging of spinal cord using q-space diffusion weighted MRI, Magn. Reson. Med. 44 (2000) 713–722.

[29] R. Nossin-Manor, R. Duvdevani, Y. Cohen, *q*-Space high *b*-value diffusion MRI of hemi-crush in rat spinal cord: evidence for spontaneous regeneration, Magn. Reson. Imaging 20 (2002) 231–241.

[30] Y. Assaf, D. Ben-Bashat, J. Chapman, S. Peled, I.E. Biton, M. Kafri, Y. Segev, T. Hendler, A.D. Korczyn, M. Graif, Y. Cohen, High *b* value *q*-space analyzed diffusion-weighted MRI: application to multiple sclerosis, Magn. Reson. Med. 47 (2002) 115–126.

[31] Y. Cohen, Y. Assaf, High *b* value *q*-space analyzed diffusion-weighted MRS and MRI in neuronal tissues—a technical review, NMR Biomed. 15 (2002) 516–542.

[32] D.G. Cory, A.N. Garroway, Measurement of translational displacement probabilities by NMR—An indicator of compartmentation, Magn. Reson. Med. 14 (1990) 435–444.

[33] J.E. Tanner, Use of stimulated echo in NMR diffusion studies, J. Chem. Phys. 52 (1970) 2523–2526.

[34] P.P. Mitra, B.I. Halpeen, Effects of finite gradient-pulse widths in the pulsed-field-gradient diffusion measurements, J. Magn. Reson. A 113 (1995) 94–101.

[35] T. Niendorf, D.G. Norris, D. Leibfritz, Detection of apparent restricted diffusion in healthy rat brain at shot diffusion time, Magn. Reson. Med. 32 (1994) 672–677.

[36] T. Niendorf, R.M. Dijkhuizen, D.G. Norris, M. van Lookeren Campagne, K. Nicolay, Biexponential diffusion attenuation in various states of brain tissue: implications for diffusion-weighted imaging, Magn. Reson. Med. 36 (1996) 847–857.

[37] G.J. Stanisz, A. Szafer, G.A. Wright, R.M. Henkelman, An analytical model for restricted diffusion in bovine optic nerve, Magn. Reson. Med. 37 (1997) 103–111.

[38] Y Assaf, Y. Cohen, Non-mono-exponential attenuation of water and *N*-acetyl aspartate signals due to diffusion in brain tissue, J. Magn. Reson. 131 (1998) 69–85.

[39] S. Peled, D.G. Cory, S.A. Raymond, D.A. Kirschner, F.A. Jolesz, Water diffusion, T2, and compartmentation in frog sciatic nerve, Magn. Reson. Med. 42 (1999) 911–918.

[40] C. Beaulieu, The basis of anisotropic water diffusion in the nervous sysyem a technical review, NMR Biomed. 15 (2002) 435–455.

[41] E.A.H. von dem Hagen, R.M. Henkelman, Orientational diffusion reflects fiber structure within a voxel, Magn. Reson. Med. 48 (2002) 454–459.